The chimera state in colloidal phase oscillators with hydrodynamic interaction

Evelyn Hamilton, Nicolas Bruot, and Pietro Cicuta

Articles you may be interested in

Coexistence between silent and bursting states in a biophysical Hodgkin-Huxley-type of model
Chaos: An Interdisciplinary Journal of Nonlinear Science **27**, 123101 (2017); 10.1063/1.4986401

Experiments with arbitrary networks in time-multiplexed delay systems
Chaos: An Interdisciplinary Journal of Nonlinear Science **27**, 121103 (2017); 10.1063/1.5016047

Robustness of coupled oscillator networks with heterogeneous natural frequencies
Chaos: An Interdisciplinary Journal of Nonlinear Science **27**, 123105 (2017); 10.1063/1.4991742

Insensitivity of synchronization to network structure in chaotic pendulum systems with time-delay coupling
Chaos: An Interdisciplinary Journal of Nonlinear Science **27**, 126702 (2017); 10.1063/1.5010304

Solitary states for coupled oscillators with inertia
Chaos: An Interdisciplinary Journal of Nonlinear Science **28**, 011103 (2018); 10.1063/1.5019792

Dynamics of delay-coupled FitzHugh-Nagumo neural rings
Chaos: An Interdisciplinary Journal of Nonlinear Science **28**, 013104 (2018); 10.1063/1.5000854

The chimera state in colloidal phase oscillators with hydrodynamic interaction

Evelyn Hamilton,[1] Nicolas Bruot,[2,a)] and Pietro Cicuta[1,b)]

[1]*Cavendish Laboratory, University of Cambridge, Cambridge CB3 0HE, United Kingdom*
[2]*Institute of Industrial Science, University of Tokyo, Tokyo, Japan*

The chimera state is the incongruous situation where coherent and incoherent populations coexist in sets of identical oscillators. Using driven non-linear oscillators interacting purely through hydrodynamic forces at low Reynolds number, previously studied as a simple model of motile cilia supporting waves, we find concurrent incoherent and synchronised subsets in small arrays. The chimeras seen in simulation display a "breathing" aspect, reminiscent of uniformly interacting phase oscillators. In contrast to other systems where chimera has been observed, this system has a well-defined interaction metric, and we know that the emergent dynamics inherit the symmetry of the underlying Oseen tensor eigenmodes. The chimera state can thus be connected to a superposition of eigenstates, whilst considering the mean interaction strength within and across subsystems allows us to make a connection to more generic (and abstract) chimeras in populations of Kuramoto phase oscillators. From this work, we expect the chimera state to emerge in experimental observations of oscillators coupled through hydrodynamic forces. *Published by AIP Publishing.*
https://doi.org/10.1063/1.4989466

A group of oscillators can form two distinct subsets—one synchronised and the other asynchronous. This state with incoherent and coherent subsets is called a chimera state and even forms when the oscillators are identical.[1] It is usually recognised by a subgroup developing disparate frequencies and losing synchrony. This unique state has been attributed to a variety of phenomena, including unihemispheric sleep cycles in birds and lizards as well as consensus in social groups.[2,3] We focus on oscillators coupled through hydrodynamic force, which is a common mechanism by which various biological systems coordinate, including motile cilia.[4] Cilia are hair-like growths of a cell, the structure of which is highly conserved across species. The coordination of motile cilia is responsible for symmetry breaking during foetal development, as well as fluid transport in the brain and lungs.[4–6] We find chimera states in simulations of small arrays of driven non-linear oscillators, which were based on motile cilia. These states are surprisingly robust, and we interpret them in terms of each subset mean interaction and by considering symmetries of the underlying interaction tensor. We expect this robustness to translate to experimental observations of the chimera state in oscillators with hydrodynamic coupling. Furthermore, the chimera state may play a part in understanding collective dynamics of motile cilia.

INTRODUCTION

Synchronisation is a general phenomenon in nonlinear dynamical systems and is connected to a breadth of applications.[7] The coordination between oscillators is an important paradigm for modelling systems across biology, physics, and chemistry: the flashing of fireflies, pendulum clocks, and the Belousov-Zhabotinsky (BZ) reaction being common examples in these disciplines.[8]

A "chimera state" is a state with simultaneous incoherent and coherent subsets, and is receiving increasing amounts of interest. It has been observed in phase, amplitude, and chaotic oscillators, using a variety of different models including Ginzburg-Landau, Kuramoto, Lorenz, Stuart-Landau, and FitzHugh-Nagumo oscillators.[9–13] The types of coupling leading to the formation of these states include uniform, nonlocal, and time-delayed interactions.[10,14,15] Though once thought to be a theoretical anomaly, it has now been observed experimentally.[16–18] The systems involved vary in terms of scale and oscillator type, with optical, chemical, and mechanical oscillators all exhibiting the chimera.[12,16–22] The state is being related to a range of natural phenomena.[1,2,23–25] It has been linked to many biological systems that involve complex and often competing interactions, from internal processes such as epilepsy and heart fibrillation to ecological predator and prey systems.[1,26–30]

Hydrodynamic interactions are common in biology and the fundamentals are well understood. An example involving these forces is motile cilia, which are highly conserved microscopic hair-like growths of cells, that push fluid and interact through hydrodynamic forces. Their oscillations are responsible for the transport of fluid in the brain, lungs, and reproductive systems of most mammals.[4,6,31]

We have worked on models of motile cilia with minimal, geometrically updated traps, where each oscillator, or rower, is a sphere driven in a low Reynolds regime, i.e., an over-damped system.[32–34] The model is designed to capture generic features of non-uniform oscillators interacting via a fluid, and arrays of oscillators can be simulated numerically.

Chimera-like features have been noted in another minimal model inspired by ciliated tissue, where the oscillators were heterogeneous.[5] In this work, we control the emergence of subsets by varying array geometries, changing the layout of identical rowers. Our numerical simulations show that for an appropriate interaction range and rower spacing, synchronised and incoherent populations coexist. For long range interaction, rowers all oscillate in-phase together, but when the range is restricted, phase-locked states are observed. We find that in an intermediate range, chimera states develop with the synchronised population's geometry depending on the system layout. The different states are considered in the context of the Oseen eigenmodes, which are derived from the fundamental interaction between rowers.[35,36] We see the chimera state is a combination of different modes and can predict its emergence by considering appropriate combinations of the normal mode relaxation rates. Alternatively, the chimera states can be interpreted using the mean interaction of each subset, emphasising the parallels with the behaviour of systems involving uniformly coupled Kuramoto phase oscillators.[14,37]

THE ROWER MODEL

Forces acting on a rower

Simple models to understand coordination of motile cilia have been proposed in the last decade and are reviewed in Ref. 4. In the rower model, a bead oscillates along x, driven by geometrically updated potential traps. We consider here the case where the driving potential is a simple power law $k x_r^{1/2}$, where x_r is the distance relative to the vertex of the side parabola. At the vertex, $x_r = 0$, the gradient of the potential diverges [see Fig. 1(a)]. To create oscillations, the trap is updated once the bead is at a distance δ from the vertex. The new potential is a reflection of previous along the central axis $x_r = A/2 + \delta$; the red and blue curves in Fig. 1(a) illustrate this. The update point δ prevents $x_r = 0$, where the force would diverge. The exponent of the power law was chosen to guarantee in-phase synchronisation between pairs of rowers and follows directly from the implementation in Ref. 38. The y position of the rowers is maintained by a harmonic trap, which depending on the row has a minimum at 0 or d_R. These traps restrict the rower oscillations to one-dimension, along the x-axis. The velocity of the ith rower is

$$\frac{d\boldsymbol{r}_i}{dt} = \sum_{j=1}^{N} \boldsymbol{H}_{ij}\boldsymbol{F}_j + \boldsymbol{f}_i, \qquad (1)$$

where $\boldsymbol{f}_i$ is a stochastic noise term, $\boldsymbol{F}_j$ is the trapping force, and $\boldsymbol{H}_{ij}$ captures the hydrodynamic interaction between the N rowers. From Brownian dynamics, the noise has zero mean and $\langle \boldsymbol{f}_i(t)\boldsymbol{f}_j(t')\rangle = 2k_B T \boldsymbol{H}_{ij}\delta(t-t')$.[39] We define the interaction tensor as

$$\boldsymbol{H}_{ij} = \begin{cases} \mathbf{I}/\gamma & : i = j \\ \dfrac{3}{4\gamma}\left(\dfrac{a}{r_{ij}}\right)^{\zeta}\left[\mathbf{I} + \hat{\mathbf{r}}_{ij}\hat{\mathbf{r}}_{ij}\right] & : i \neq j \end{cases}, \qquad (2)$$
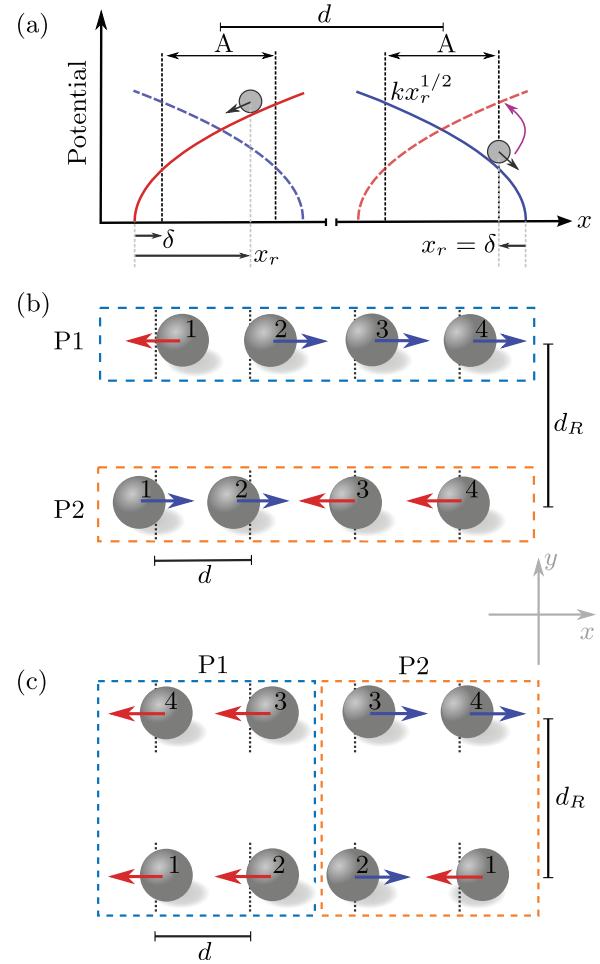

FIG. 1. Rowers are a simple model for non-uniform oscillators that interact at low Reynolds number. (a) Beads are driven by a power law potential $k x_r^{1/2}$, where x_r is the distance relative to the trap vertex. Once a rower is δ from its vertex, its trap switches (continuous to dashed potential in diagram). The diagram illustrates two rowers, and each oscillates with amplitude A. More complex arrays can be made, and we focus on systems of eight beads. (b) and (c) Beads are placed in two rows. Within a row, the trap centres are spaced d apart. The two rows are separated by d_R. Depending on the spacing and interaction, the dynamics of the rowers tend to divide into block or chain populations. The chain is shown in (b), and the block is shown in (c). The two populations are labelled P1 and P2, with blue and orange rectangles marking the appropriate subset. The rowers are numbered in the block or chain configuration to ensure that the central beads are always indexed 2 and 3.

where $\gamma = 6\pi\eta a$ is the drag (η is the viscosity of the fluid), and $\hat{\mathbf{r}}_{ij}$ and r_{ij} are the direction and distance between rowers. The parameter ζ is introduced as a simple control for the interaction range and takes some value between $[1, 3]$. In the far-field limit when the rower radius a is much smaller than the distance separating them and $\zeta = 1$, $\boldsymbol{H}_{ij}$ is the Oseen tensor. At the other extreme where $\zeta = 3$, $\boldsymbol{H}_{ij}$ is akin to the limit of the Blake tensor near a wall. The interval of ζ creates an interaction decay rate somewhere between being far from any impediment ($\zeta = 1$) and being near a no-slip boundary ($\zeta = 3$). The tensor allows the coupling between the rowers to be altered in two ways. Changing ζ from 1 to 3 increases the decay of the interaction, so the rowers no longer interact over a long range but only with their close neighbours. The second way to adjust the coupling is to vary the distance between rowers. The rowers are arranged to encourage

separation into two subsets, with the eight beads placed in two rows as shown in Fig. 1(b). To alter the coupling through position, the distance between the rows d_R is varied.

Preferred population configuration

The rowers tend to synchronise in either chain or block configurations. Examples of the two geometries are shown in Figs. 1(b) and 1(c). The chain configuration is shown in 1(b), with the first population (P1) marked in blue and the second (P2) marked in orange. Blue and orange also indicate P1 and P2 for the block configuration in Fig. 1(c). The choice of most natural subset depends on the interaction range and the distance between the rows d_R.

The simulation parameters are chosen to produce strong interactions between the rowers. We want high negative curvature, as defined in Ref. 38, and low noise. This ensures strong in-phase synchronisation between a pair of rowers, so any departure from this state is the result of additional rowers. The curvature depends on the force at the beginning and end of the trap, F_b and F_e, as well as the average force F_0. Explicitly $c = -2(F_e - F_b)/F_0$, with $F_b = -k/2 (A + \delta)^{-1/2}$ and $F_e = -k/2 \, \delta^{-1/2}$. We set $A/\delta = 31$, which results in a curvature of $c = -0.7$ for our trap potential.

Synchronisation between a pair of rowers in the presence of noise was also explored in Ref. 38. We define the noise strength ξ in a similar way, but also include the dimensionless quantity D_0. This term scales the trap strength to maintain a given period for a chain of four rowers moving in-phase when the coupling range is varied by ζ.[40] We relate the noise to D_0, the temperature T, and average trap force F_0 by

$$\xi = \frac{2k_BT}{AD_0F_0}, \quad F_0 = \frac{1}{2}(F_e + F_b), \quad (3)$$

with A the amplitude of the oscillations and k_B the Boltzmann constant. The coupling is anisotropic in our system due to its dependence on the direction of oscillation and the geometry of the system. We compare the noise to the interaction forces along x and y by scaling it using the nearest neighbour coupling in each direction. The scaled noises for x and y, ξ_x and ξ_y, are related to ξ by

$$\xi_x = \frac{2}{3}\left(\frac{d}{a}\right)^\zeta \xi, \quad \xi_y = \frac{4}{3}\left(\frac{d_R}{a}\right)^\zeta \xi. \quad (4)$$

We set the ratio $d/a = 6.86$, and $d_R/a \in [6.86, 22.86]$, which results in $d_R/d \in [1, 3.33]$. The dimensionless trap strength is $D_0 k\tau/(\gamma a^{3/2}) = 3.28$, where τ is the period of a single chain of four rowers moving in-phase, and $\delta/a = 0.057$. Unless stated otherwise, the noise is $\xi = 2.13 \times 10^{-5}$, i.e., the noise is small when compared with the neighbouring interaction in x, with $\max(\xi_x) = 4.58 \times 10^{-3}$. ξ_x lies within the expected synchronised region[38] when the results are rescaled appropriately. This noise should not prevent the rowers coordinating with their neighbours along x. The coupling strength of vertically opposite rowers has a wider range, as both d_R and ζ vary [see Fig. 2(a)]. While the noise is initially small with $\xi_y \approx 10^{-4}$, for larger d_R/a and ζ, the noise could prevent
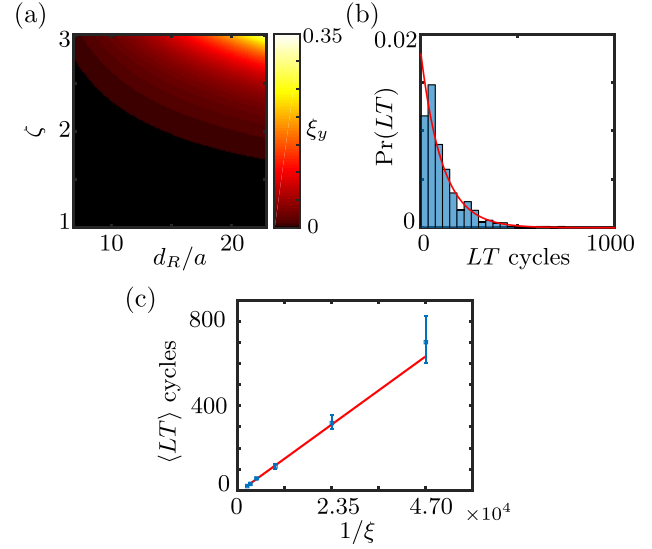

FIG. 2. The low noise level $\xi = 2.13 \times 10^{-5}$ generally does not impede the interaction in y and produces chimera states with a long lifetime. (a) The map of dimensionless noise scaled by the interaction in y, ξ_y, for varying ζ and d_R/a when $\xi = 2.13 \times 10^{-5}$. For the most part, the noise is small $\xi_y < 0.1$, with $\xi_y \approx 0.1$ the bright red. (b) The histogram of the simulated lifetime LT measurements, with the fitted distribution shown in red, when $\xi = 1.06 \times 10^{-4}$. (c) The relationship between average lifetime $\langle LT \rangle$ and $1/\xi$ is linear when $\zeta = 1.6$ and $d_R/a = 9.1$. The error bars indicate the 95% confidence interval for the mean, determined using the pivotal quantity for an exponential distribution. The fit suggests that the block chimera state is stable when noise is not present.

coordination between the rows with $\xi_y \approx 10^{-1}$. For the most part, ξ_y is small and the rower interaction along y exceeds the noise.

Details of simulation

We simulated the rowers using the method of Ermak and McCammon.[39] The Brownian noise has zero mean and is correlated by $\langle f_i(t)f_j(t') \rangle = 2k_BTH_{ij}\delta(t - t')$. When numerically solving, we used a time step equivalent to 1×10^{-4} s. The simulations were run for 1000 cycles unless investigating the lifetime. When measuring the lifetime, the simulations were run for 2000 cycles and then reseeded until at least 150 lifetimes were measured. The initial rower positions were randomly drawn from a uniform distribution $U(-A/2, A/2)$, with no preference in the initial trap orientation. To link with motile cilia and experimental work, we set the bead radius to $a = 1.75 \, \mu$m, the drag to $\gamma = 0.073$ Pa $\cdot$ s $\cdot \mu$m, and the period to $\tau = 0.49$ s; τ is the period of a single chain of four rowers.

When classifying the simulations, the results are separated into 40 cycle intervals. The first interval is discounted as the rowers start from a random position. The mean and variation of the order parameter in the remaining intervals is used to categorise the simulation results.

Measures for order

The positions of the rowers oscillate in our system. To highlight the repetitive nature of the motion, the distance is mapped to a phase or "angle" ϕ, a common approach in cyclic systems.[8] To determine the mapping, we adapted the

transformation to natural angles to account for the trap switching. This defines the phase in such a way that it grows linearly for a single rower. The explicit relation between the phase and position is $\phi(t) = N_s(t)\pi + \psi[x_r(t)]$ with $\psi(x) \propto x^{3/2}$;[41] $N_s(t)$ is the number of switches undergone by a rower at time t; $N_s(0) = 1$ if the trap starts on the left. The phase is used to determine two complex order parameters, which distinguish between different states

$$Z^{(p)}(t) = \frac{1}{N_p} \sum_{j=1}^{N_p} \exp\left[i\phi_j^{(p)}(t)\right], \qquad (5)$$

$$Z_{PL}^{(p)}(t) = \frac{1}{N_p - 1} \sum_{j=1}^{N_p - 1} \exp\left[i(\phi_{j+1}^{(p)}(t) - \phi_j^{(p)}(t))\right], \quad (6)$$

where $p = 1, 2$ labels the two populations, so $\phi_j^{(p)}$ is the phase of jth in the pth population and N_p is the size of the population. $Z^{(p)}$ is a measure of a population's mean phase, and $Z_{PL}^{(p)}$ is the measure for mean phase-difference. The magnitudes of $Z^{(p)}$ and $Z_{PL}^{(p)}$ gauge the coherence of a population, with $|Z_{PL}^{(p)}|$ measuring the variability in the phase-difference between neighbours and $|Z^{(p)}|$ measuring how in-phase the rowers are in each population. The population is incoherent when $|Z_{PL}| \approx 0$ and phase-locked (constant phase-difference) when $|Z_{PL}| \approx 1$. $|Z| \approx 1$ corresponds to the specific case when the phase-difference is zero, but $|Z| \approx 0$ occurs for both incoherent and splay states; the splay state for four

rowers is $\phi_{i+1}^{(p)}(t) - \phi_i^{(p)}(t) = \frac{\pi}{2}$. We use both measures to classify the system.

RESULTS

The interaction range ζ and row spacing d_R determine the rowers' behaviour. There are three states observed: in-phase, chimera, and phase-locked. The chimera state has two sub-categories—chimera-block and chimera-chain—depending on the subset geometry. Figure 3 shows some examples of these behaviours. When the interaction is long ranged with ζ near one, there is no separation into subsets as all the rowers oscillate in-phase. The synchronisation of the rowers when $\zeta = 1.1$ and $d_R/a = 8$ is shown in Figs. 3(a) and 3(b). It appears as vertical bands in the phase in Fig. 3(a) and the convergence to one in Fig. 3(b). When the interaction is short ranged, the oscillators settle into phase-locked states. This appears as diagonal bands in the phase and $|Z_{PL}| \approx 1$ [see Figs. 3(g) and 3(h)], where $\zeta = 3$ and $d_R/a = 21.71$. The total interaction $\sum_{i \neq j} H_{ij}^x$ tends to be weaker in these cases, and so the rowers take longer to become coordinated. The chimera state occurs in the intermediate range between the in-phase and phase-locked states. In this state, one population is in-phase, whilst the other is unable to settle with defects developing whenever it approaches in-phase. This causes $|Z|$ to rise and fall in the incoherent population. The phase defects in the chimera state when $\zeta = 1.6$ and $d_R/a = 10.28$ are shown in Figs. 3(d) and 3(e). The defects create
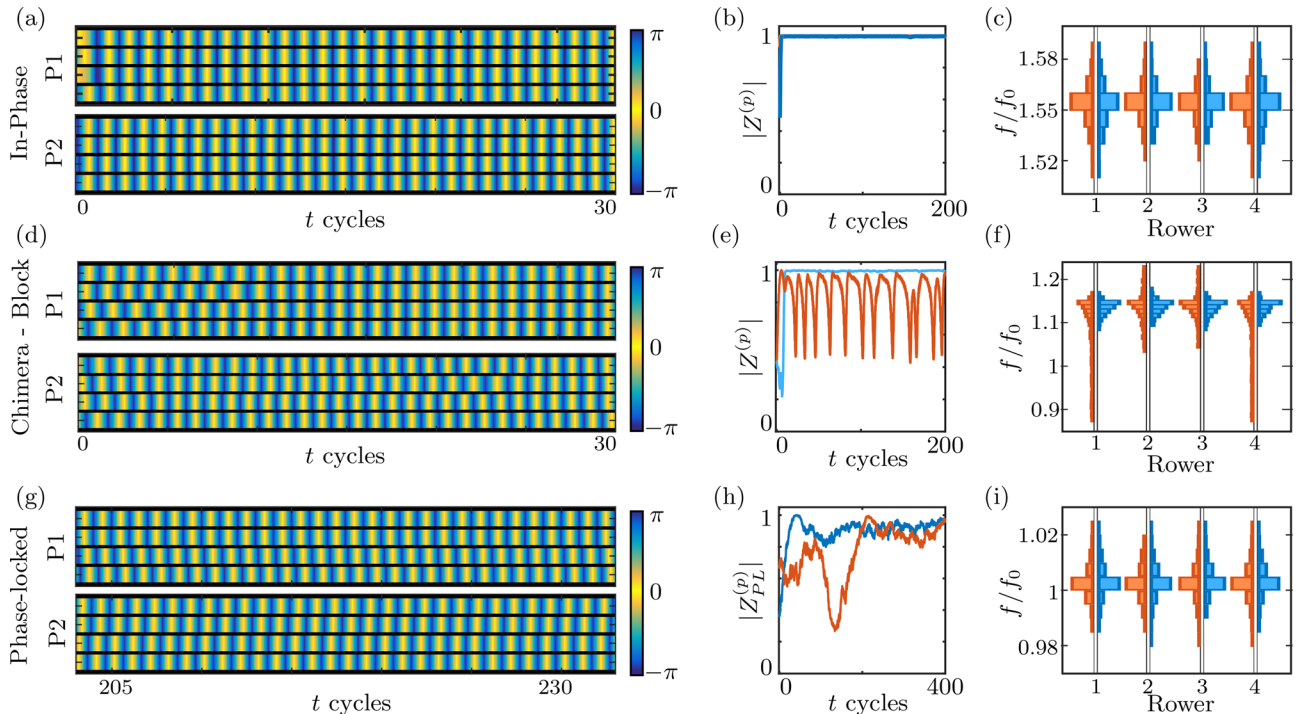

FIG. 3. The chimera state forms in the intermediate range between in-phase motion and phase-locked states. (a) and (b) The phase and order of an in-phase state, where $d_R/a = 8$ and $\zeta = 1.1$. The rowers start from a random position, but both populations (P1-blue and P2-orange) quickly form and maintain the in-phase state with $|Z^{(p)}| = 1$. (c) The frequency distributions are similar for both populations when in-phase. The distributions are horizontal, contrasting the "same" rower in each population, i.e., same number or relative position. For each rower the distribution is scaled by f_0, the frequency of a rower without interaction. (d)–(f) Only one population can coordinate when $d_R/a = 10.29$ and $\zeta = 1.6$. Defects develop in pairs of rowers from the second population P2, preventing in-phase motion. The defects result in apparent 'breathing' in the orange curve of the order parameter and a tail developing in the frequency distribution. The skew is responsible for the drop in mean frequency, behaviour associated with the chimera state. (g)–(i) For a sufficiently short interaction range, the phase-locked state occurs, $d_R/a = 21.71$ and $\zeta = 3$. The total strength of the interacting forces is smaller for short ranged interactions, so the rowers are slow to settle into the phase-locked state.
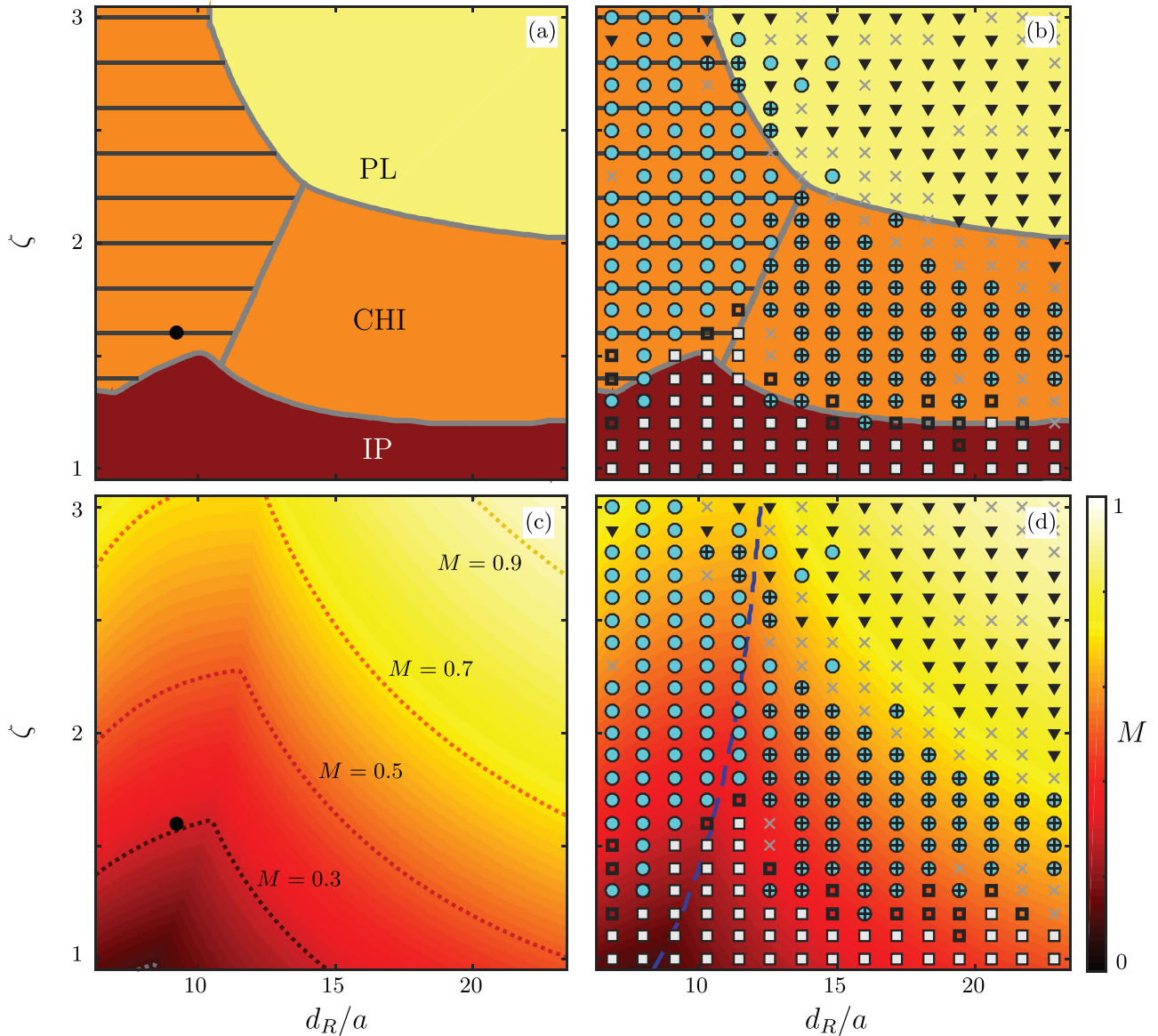
FIG. 4. Regions for the different states can be classified using the growth rate or the difference between intra- and cross- population forces. (a) and (b) The classification of the different regions using the eigenmode growth rates G_j: the in-phase region (burgundy), phase-locked region (yellow), and the chimera region between (orange). The in-phase state is observed when the growth rate of the in-phase eigenmode G_1 outstrips the others. We define the in-phase section by $G_4 < 0.125$ and $G_2 - G_4 > 0.012$, which ensures that the growth rates of the other states are small; G_j are indexed in descending size. Phase-locking occurs when all the growth rates converge. The region where the rates have coalesced is defined by the faster growth rates being similarly spaced to the slower, more closely spaced states, $G_1 - G_2 < G_5 - G_7$ and $G_1 - G_3 < G_4 - G_7$. The stripes mark when the block formation is preferred to the chain. This region is defined by $G_2 - G_3 < G_4 - G_5$, i.e., using the slower states to determine when the difference in growth between chain and block states is small. (c) and (d) The colour indicates the difference in population forces, $M = (\mu - \nu)/(\mu + \nu)$. Lines for $M = 0.3$, 0.5, 0.7, and 0.9 are plotted and labelled. The cusp in the lines indicates where the rowers swap from preferring block configuration to chain. The cusp is marked by a dashed line in (d), i.e., the expected transition point from block to chain. (b) and (d) The results of simulation are superimposed over the different regions. White squares, cyan circles, and black triangles mark in-phase, chimera, and phase-locked states. A grey cross indicates the state could not be classified, whilst an open square marks a mixture of in-phase and chimera behaviour. To distinguish the chain-chimera, a plus is added to the cyan circle. The lifetime stability for the block-chimera was measured at the dark point in (a) and (c), where $\zeta = 1.6$ and $d_R/a = 9.14$.

the apparent "breathing" in the order parameter $|Z|$ of the unsynchronised population. The frequency distributions of phase-locked and in-phase states are symmetric, but the distribution of incoherent rowers develops a tail [see Figs. 3(c), 3(f), and 3(g)]. This leads to a reduction in mean frequency for the unsynchronised population in the chimera state.

When noise is present, the subsets do swap roles, but as the noise decreases the chimera intervals last for longer periods. When comfortably within the chimera-block region [see

the circle marker in Figs. 4(a) and 4(c)], the lifetime of the state increases linearly with $1/\xi$ (see Fig. 2). Although the lifetime of the chain state increases with decreasing noise, it also exhibits chaotic characteristics. This makes it difficult to make definitive claims concerning the long term behaviour. Since we are interested in a physical system with noise, we classify the chimera state by considering 40 cycle intervals. When more than half the intervals measure one population remain synchronised whilst the other fluctuates, the state is

labelled as a chimera. The states are classified as block or chain by comparing $|Z|$ for both configurations; it is then categorised as the geometry that measures a different spread in $|Z|$ for each population.

MEAN INTERACTION

The observed chimera state, particularly the rise and fall in incoherent population mentioned in the Results section, is reminiscent of the "breathing" seen in populations of Kuramoto phase oscillators.[14,37] The Kuramoto populations are uniformly coupled, suggesting that the mean population forces encapsulate the chimera behaviour. To parallel this work, we consider the difference between the mean couplings within each subset M

$$M = \frac{\mu - \nu}{\mu + \nu}, \qquad (7)$$

$$\mu = \sum_{\substack{j \neq 1 \\ j \in P_1}} H_{1j}^x, \quad \nu = \sum_{j \in P_2} H_{1j}^x, \qquad (8)$$

where μ is the sum of forces parallel along x within a population acting on a bead labelled as number one in Fig. 1. The mean cross population force ν is the sum of forces on the same rower exerted by the other population. Using the mean interaction, we find that our results are reconcilable with the Kuramoto oscillators, and the transition from block to chain subsets can be predicted.

In-phase behaviour is expected when M is small, and the cross-population forces are comparable to intra-population, i.e., $\zeta \approx 1$, and forces are long-range. In contrast, the mean interaction becomes a poor approximation for the dynamics when the interactions are short range, particularly for the chain configuration, where the difference between maximum and minimum spacing is larger. The effect of varying ζ and d_R on M is shown in Figs. 4(c) and 4(d). The expected shift from block to chain is at the cusp in the M curves. It occurs when the chain population sum μ_C exceeds the block μ_B. The chain population's enhanced sensitivity to ζ is also apparent, seen as the section of high M when d_R increases and $3 > \zeta > 2$. Simulation results are overlaid in the map of M in Fig. 4(d). The different markers in Fig. 4(d) correspond to the in-phase, chimera, and phase-locked states. The chain-chimera states are marked with a plus. A mixture of chimera and in-phase is recorded when over half the simulation registers in-phase motion but there is an interval of chimera behaviour, and shown by the empty squares. If the simulation does not measure consistent high levels of $|Z_{PL}|$ in either population, then it is not classified and is marked by a grey cross. The cusp in M occurs on the navy line. The chain states begin to be observed when $\mu_C > \mu_B$. More generally, the chimera state is recorded when $0.7 > M > 0.4$. The upper bound results from the shortened interaction range, whilst the lower bound is consistent with Ref. 37. There is no direct correspondent for the phase lag from the Kuramoto model, but the boundary near 0.4 is in accord with a moderate range of phase lag. For small d_R, the intra-population forces are more uniform, so the map of M best captures

results that occur in this range. In particular the dark patch where $M < 0.25$, when $6.8 < d_R/a < 11.5$, captures the transition from in-phase to block chimera behaviour.

Given its small size, our chimera is surprisingly stable. Particularly when contrasted with the uniformly interacting Kuramoto oscillators.[42] The chimera states observed in small numbers of BZ oscillators were also noted to be oddly stable, as were small networks of amplitude-phase coupled lasers.[17,43] Their stability was attributed to the differences between them and simple phase oscillators. The geometric updating traps of the rower model may be producing a similar stabilising effect here. This stability would translate to experimental realisations of rower systems and could have biological relevance in ciliated tissues.

THE EIGENMODES

Eigenstate growth rate

The behaviour of rower ensembles can be understood qualitatively from their fundamental interaction by projecting onto appropriate eigenstates. This technique has previously been applied to rings of rowers,[36] two rows of rowers with varying oscillation direction,[44] and a similar approach has been used to understand synchronisation in quantum oscillators coupled through dissipation.[45,46] Following the procedure in Ref. 36, where the distance between the rowers r_{ij} is approximated by the distance between their trap centres (a function of d and d_R) and noise is neglected, the system configuration at each time can be projected onto the eigenvectors of the interaction tensor. To express the trap force in terms of the projection, the potential needs to be parabolic. Earlier work in Ref. 38 showed that rower synchronisation is governed by the curvature of the potential. Consequently we use a negative parabolic potential with the same curvature as the earlier square root form to calculate the eigenmodes, i.e., the potential $-k_p x_p^2$ with $\delta_p/a = 0.37$ [see Fig. 5(a)]. To match the $x_r^{1/2}$ potential, the parabolic trap strength is set by $k_p = k\left(\sqrt{A + \delta} - \sqrt{\delta}\right)/((A + \delta_p)^2 - \delta_p^2)$. In shifting to the new potential, the distance is now measured relative to the turning point of the parabola. The new potential means $h_j = \hat{e}_j \cdot r$, the projection of the rower positions onto the jth eigenvector, obeys

$$h_j(t) - (\hat{e}_j \cdot s) - \tau_j \frac{d}{dt} h_j(t) = 0, \qquad (9)$$

$$\tau_j = \frac{\gamma/(2k_p)}{1 + \frac{3}{4}(a/d)^\zeta \lambda_j}, \qquad (10)$$

where λ_j is the eigenvalue associated with the vector, s the trap position vector, and k_p the trap strength for the parabolic potential. This expression only holds between trap updates, i.e., s is constant.

Employing a similar argument as that in Ref. 36, but focused on divergence, predicts that the observed state will be the fastest diverging state because the state that diverges fastest experiences the greatest growth between trap updates. Using the approximation of a parabolic potential, the growth rate of the jth mode over one switch G_j is
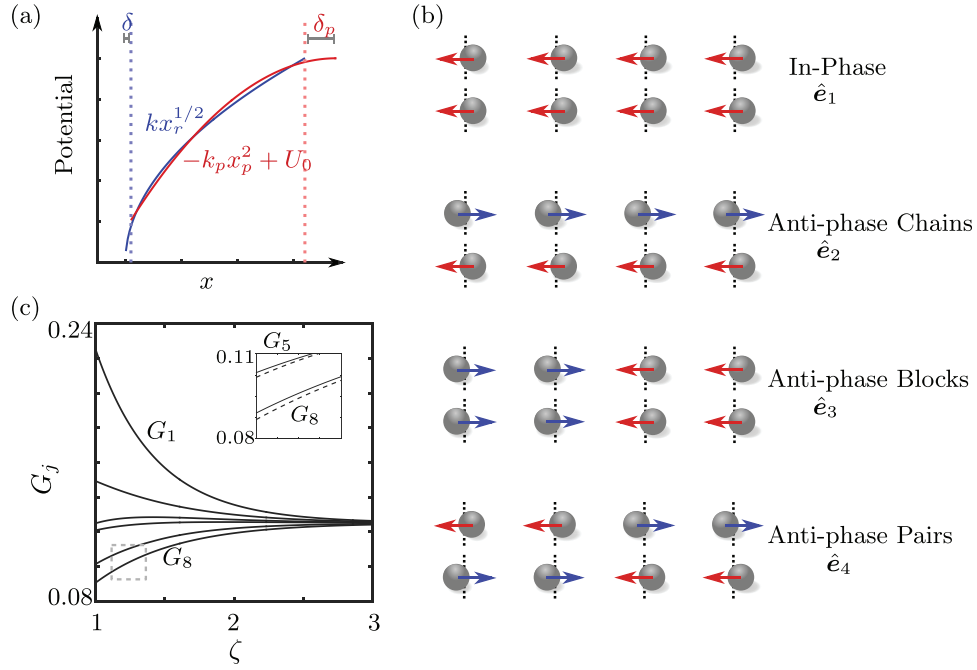
FIG. 5. The growth rate of the interaction tensor's eigenstates G_j when the trap potential is parabolic. (a) Approximating the original $x^{1/2}$ potential with a negative parabola that maintains the curvature. The original potential is shown in blue, and the new parabolic potential is in red. The parabola has been translated by U_0 to highlight the similarity to $kx_r^{1/2}$, but the force is unaffected by this value. (b) Representations of four eigenstates states. In-phase motion or $\hat{e}_1$ grows the fastest, followed by $\hat{e}_2$ anti-phase chain population, $\hat{e}_3$ anti-phase block populations, and $\hat{e}_4$ anti-phase pairs. (c) The growth rate of the different eigenstates assuming the rowers are either phase-locked or in the chimera state, i.e., $n_t = 5$, with $d_R/a = 10.29$. The growth rate is indexed by descending size, so G_1 is the fastest rate and G_8 the slowest. The difference between G_5 and G_6 and G_7 and G_8 is minimal, so only one of each pair is considered when classifying the states. These states are shown in the inset, which is a closer view of the dashed section in the lower left corner.

$$G_j = \frac{\exp\left[t_s/(n_t\tau_j)\right] - 1}{\sum\limits_{k=1}^{N}\{\exp[t_s/(n_t\tau_k)] - 1\}}. \tag{11}$$

The growth is measured over the median time between any two switches t_s/n_t, with t_s the time between a rower's switches and n_t the median number of traps expected to update over this period. The switch time is interpolated from the simulation results, as are the number of switches. When in-phase $n_t = 1$, and for the chimera and phase-locked states, $n_t = 5$. Each state will be diverging, but the system prefers the state which diverges the quickest. The index j orders the states by their rate of divergence, and G_1 is the fastest growth while G_8 is the slowest. The four states fastest to diverge are in-phase, anti-phase chain, anti-phase block, and anti-phase pairs. Representations of these four states are shown in Fig. 5(b).

The growth rates when $n_t = 5$ are plotted against the interaction range ζ for the different states in Fig. 5(c). These growth rates were used when classifying the different regions for the behaviour. The general trend when ζ increases is for the states to converge to equal representation (1/8). The inset zooms in on G_5, G_6, G_7, and G_8. The difference between G_5 and G_6 (and G_7 and G_8) is small; as such, there are only six states well separated. We classify the regions using the well separated states G_1, G_2, G_3, G_4, G_5, and G_7.

Classification using growth rate

The in-phase motion is associated with the fastest diverging state, while the phase-locked state is a sequence of states involving combinations of all the different eigenstates. The in-phase state occurs when a single growth rate exceeds others, whilst the phase-locked state is observed once all the rates have converged. The chimera state occurs in the range between, where the in-phase growth no longer dominates, but all the states have yet to converge.

We expect the rowers to be in-phase when G_1 is much larger than the other rates. We find the in-phase region to be the intersection of $G_4 < 0.125$ and $G_2 - G_4 > 0.012$. The eight eigenstates mean equal representation occurs at $G_j = 0.125$, with G_1, G_2, G_3, G_4 approaching this limit from above and G_5, G_6, G_7, G_8 from below. The in-phase boundary conditions ensure that all but the fastest state must be clustered at their minimum value. This is the dark region shaded in Fig. 4. To find the phase-locked boundary, the growth rates need to be comparable. The region is found as $G_1 - G_2 < G_5 - G_7$ and $G_1 - G_3 < G_4 - G_7$, i.e., using the more closely spaced, slow growth rates as the threshold for the faster rates converging. This is the pale yellow region marked in Fig. 4. The chimera occurs between these regions, with the transition between block and chain geometries reflecting a reduction in the coupling between the rows. Increasing d_R, i.e., decoupling the rows, causes anti-phase row states to converge (e.g., $\hat{e}_1$ and $\hat{e}_2$, or $\hat{e}_3$ and $\hat{e}_4$). As with the phase-locked state, the difference between the slower states was used as the benchmark for similarity. We find the block region to be $G_2 - G_3 < G_4 - G_5$, which ensures that the difference between the block and chain growth is comparatively small. This implies that the row coupling is still strong, and as such the block geometry develops.

The simulation results are superimposed over the original image in Fig. 4(b). White square, cyan circles, and black triangles indicate in-phase, chimera, and phase-locked states. The chain-chimera sub-category is marked by the addition of a plus to the cyan circle. States unable to be classified are indicated by a grey cross, and states that are a mixture of chimera and in-phase are indicated by open squares. The growth rate captures the rowers' behaviour well for large d_R, but some features are missing at lower d_R.

The in-phase boundary intersects with the states exhibiting a mixture of chimera and in-phase behaviour (open circles) but misses some in-phase states near $d_R/a \approx 10.3$. Similarly the phase-locking border passes through the unclassified states (grey crosses) at large d_R, but there are a mixture of phase-locked and block-chimera included by the border at small d_R. The block boundary covers most block states, but there are some inconsistencies for particularly short ranged interactions. The success of the growth rate boundaries is a good indicator that the chimera state involves a mixture of $\hat{e}_1$, $\hat{e}_2$, $\hat{e}_3$, and $\hat{e}_4$ but is less clear on the exact combination.

CONCLUSION

We find the chimera state using simulations of a simple model for non-uniform oscillators with a hydrodynamic interaction. The resulting states can be interpreted using the eigenmodes of the interaction tensor and their associated growth rates. Specifically the chimera state appears when the faster growth rates have converged but not with the slower states. The faster states converging means combination of these states is not suppressed, and the system separates into two subsets. This gives rise to the synchronised and incoherent subsets expected of the chimera state. Alternatively, the system can be analysed by assuming the existence of two subsets and considering their mean interaction. This simple approach links the rower chimera state results to chimera states in Kuramoto oscillators. Additionally, the mean interaction predicts the shift in preferred population geometry from block to chain by comparing the intra-population forces for each geometry. In contrast to the eigenmodes whose growth rates suggest which eigenstates govern the chimera, the mean interaction is a simple indicator of which geometry is preferred.

In conclusion, we have simulated the chimera state using a simple, minimal model for non-linear oscillators interacting at low Reynolds number. We would expect this to emerge in experimental observations of the chimera state in oscillators with hydrodynamic coupling, and it may play a part in understanding collective dynamics of motile cilia.

ACKNOWLEDGMENTS

[1]M. J. Panaggio and D. M. Abrams, "Chimera states: Coexistence of coherence and incoherence in networks of coupled oscillators," Nonlinearity **28**, R67 (2015).

[2]R. Ma, J. Wang, and Z. Liu, "Robust features of chimera states and the implementation of alternating chimera states," Europhys. Lett. **91**, 40006 (2010).

[3]J. González-Avella, M. Cosenza, and M. San Miguel, "Localized coherence in two interacting populations of social agents," Physica A **399**, 24–30 (2014).

[4]N. Bruot and P. Cicuta, "Hydrodynamically coupled driven colloidal oscillators as models of motile cilia synchronization and cooperation," Annu. Rev. Condens. Matter Phys. **7**, 323–348 (2016).

[5]D. R. Brumley, N. Bruot, J. Kotar, R. E. Goldstein, P. Cicuta, and M. Polin, "Long-range interactions, wobbles and phase defects in chains of fluid-coupled oscillators," Phys. Rev. Fluids **1**, 081201 (2016).

[6]M. Fliegauf, T. Benzing, and H. Omran, "When cilia go bad: Cilia defects and ciliopathies," Nat. Rev. Mol. Cell Biol. **8**, 880–893 (2007).

[7]S. Strogatz, *Nonlinear Dynamics and Chaos: With Applications to Physics, Biology, Chemistry, and Engineering*, Advanced Book Program (Westview Press, 1994).

[8]M. G. Rosenblum, A. Pikovsky, and J. Kurths, *Synchronization – A Universal Concept in Nonlinear Sciences* (Cambridge University Press, Cambridge, 2001).

[9]Y. Kuramoto and D. Battogtokh, "Coexistence of coherence and incoherence in nonlocally coupled phase oscillators," Nonlinear Phenom. Complex Syst. **5**, 380–385 (2002).

[10]D. M. Abrams and S. H. Strogatz, "Chimera states for coupled oscillators," Phys. Rev. Lett. **93**, 174102 (2004).

[11]R. Gopal, V. K. Chandrasekar, A. Venkatesan, and M. Lakshmanan, "Observation and characterization of chimera states in coupled dynamical systems with nonlocal coupling," Phys. Rev. E **89**, 052914 (2014).

[12]L. Schmidt, K. Schönleber, K. Krischer, and V. García-Morales, "Coexistence of synchrony and incoherence in oscillatory media under nonlinear global coupling," Chaos **24**, 013102 (2014).

[13]A. Zakharova, M. Kapeller, and E. Schöll, "Chimera death: Symmetry breaking in dynamical networks," Phys. Rev. Lett. **112**, 154101 (2014).

[14]D. M. Abrams, R. Mirollo, S. H. Strogatz, and D. A. Wiley, "Solvable model for chimera states of coupled oscillators," Phys. Rev. Lett. **101**, 084103 (2008).

[15]G. C. Sethia, A. Sen, and F. M. Atay, "Clustered chimera states in delay-coupled oscillator systems," Phys. Rev. Lett. **100**, 144102 (2008).

[16]A. M. Hagerstrom, T. E. Murphy, R. Roy, P. Hövel, I. Omelchenko, and E. Schöll, "Experimental observation of chimeras in coupled-map lattices," Nat. Phys. **8**, 658–661 (2012).

[17]M. R. Tinsley, S. Nkomo, and K. Showalter, "Chimera and phase-cluster states in populations of coupled chemical oscillators," Nat. Phys. **8**, 662–665 (2012).

[18]E. A. Martens, S. Thutupalli, A. Fourrière, and O. Hallatschek, "Chimera states in mechanical oscillator networks," Proc. Natl. Acad. Sci. U.S.A. **110**, 10563–10567 (2013).

[19]P. Ashwin and O. Burylko, "Weak chimeras in minimal networks of coupled phase oscillators," Chaos **25**, 013106 (2015).

[20]A. Röhm, F. Böhm, and K. Lüdge, "Small chimera states without multistability in a globally delay-coupled network of four lasers," Phys. Rev. E **94**, 042204 (2016).

[21]S. Nkomo, M. R. Tinsley, and K. Showalter, "Chimera and chimera-like states in populations of nonlocally coupled homogeneous and heterogeneous chemical oscillators," Chaos **26**, 094826 (2016).

[22]K. Blaha, R. J. Burrus, J. L. Orozco-Mora, E. Ruiz-Beltrán, A. B. Siddique, V. D. Hatamipour, and F. Sorrentino, "Symmetry effects on naturally arising chimera states in mechanical oscillator networks," Chaos **26**, 116307 (2016).

[23]D. Barkley and L. S. Tuckerman, "Computational study of turbulent laminar patterns in Couette flow," Phys. Rev. Lett. **94**, 014502 (2005).

[24]C. R. Laing and C. C. Chow, "Stationary bumps in networks of spiking neurons," Neural Comput. **13**, 1473–1494 (2001).

[25]N. Rattenborg, C. Amlaner, and S. Lima, "Behavioral, neurophysiological and evolutionary perspectives on unihemispheric sleep," Neurosci. Biobehav. Rev. **24**, 817–842 (2000).

[26]A. V. Panfilov, "Spiral breakup as a model of ventricular fibrillation," Chaos **8**, 57–64 (1998).

[27]R. G. Andrzejak, C. Rummel, F. Mormann, and K. Schindler, "All together now: Analogies between chimera state collapses and epileptic seizures," Sci. Rep. **6**, 23000 (2016).

[28]T. Banerjee, P. S. Dutta, A. Zakharova, and E. Schöll, "Chimera patterns induced by distance-dependent power-law coupling in ecological networks," Phys. Rev. E **94**, 032206 (2016).

[29]E. A. Martens, C. R. Laing, and S. H. Strogatz, "Solvable model of spiral wave chimeras," Phys. Rev. Lett. **104**, 044101 (2010).

[30]T. Xiaodong, Y. Tao, I. R. Epstein, L. Yang, Z. Yuemin, and G. Qingyu, "Novel type of chimera spiral waves arising from decoupling of a diffusible component," J. Chem. Phys. **141**, 024110 (2014).

[31]A. E. Tilley, M. S. Walters, R. Shaykhiev, and R. G. Crystal, "Cilia dysfunction in lung disease," Annu. Rev. Physiol. **77**, 379–406 (2015).

[32]M. C. Lagomarsino, B. Bassetti, and P. Jona, "Rowers coupled hydrodynamically: Modeling possible mechanisms for the cooperation of cilia," Eur. Phys. J. B **26**, 81–88 (2002).

[33]M. Leoni, B. Bassetti, J. Kotar, P. Cicuta, and M. C. Lagomarsino, "Minimal two-sphere model of the generation of fluid flow at low Reynolds numbers," Phys. Rev. E **81**, 036304 (2010).

[34]J. Kotar, M. Leoni, B. Bassetti, M. C. Lagomarsino, and P. Cicuta, "Hydrodynamic synchronization of colloidal oscillators," Proc. Natl. Acad. Sci. U.S.A. **107**, 7669–7673 (2010).

[35]G. M. Cicuta, J. Kotar, A. T. Brown, J.-H. Noh, and P. Cicuta, "Hydrodynamic coupling in polygonal arrays of colloids: Experimental and analytical results," Phys. Rev. E **81**, 051403 (2010).

[36]G. M. Cicuta, E. Onofri, M. C. Lagomarsino, and P. Cicuta, "Patterns of synchronization in the hydrodynamic coupling of active colloids," Phys. Rev. E **85**, 016203 (2012).

[37]M. J. Panaggio, D. M. Abrams, P. Ashwin, and C. R. Laing, "Chimera states in networks of phase oscillators: The case of two small populations," Phys. Rev. E **93**, 012218 (2016).

[38]N. Bruot, J. Kotar, F. de Lillo, M. C. Lagomarsino, and P. Cicuta, "Driving potential and noise level determine the synchronization state of hydrodynamically coupled oscillators," Phys. Rev. Lett. **109**, 164103 (2012).

[39]D. L. Ermak and J. A. McCammon, "Brownian dynamics with hydrodynamic interactions," J. Chem. Phys. **69**, 1352–1360 (1978).

[40]$D_0 = 1 + \frac{3}{2}\left(\frac{a}{d}\right)^{\zeta}\Lambda$, where Λ is the largest eigenvalue of $(\boldsymbol{I} + \hat{\mathbf{r}}_{ij}^{(c)}\hat{\mathbf{r}}_{ij}^{(c)})$ when $\hat{\mathbf{r}}_{ij}^{(c)}$ is the distance between rowers in a chain. It was assumed the rowers were spaced parallel to their oscillation direction. We limit the chain to four rowers. The formula is an adaptation of relaxation time in Eq. (5) of Ref. 36.

[41]The explicit formula for the linear phase is $\psi(x_r) = -\frac{\gamma\Omega}{1/2k}\frac{2}{3}x_r^{3/2} + \psi_0$, where Ω is the angular frequency of a single rower $\Omega = 2\pi f_0$ and the frequency depending on the switch time $f_0 = 1/(2t_s)$. ψ_0 is a constant that sets the phase of the rower to 0 at the switch point, i.e. $\psi(\delta) = 0$.

[42]M. Wolfrum and O. E. Omel'chenko, "Chimera states are chaotic transients," Phys. Rev. E **84**, 015201 (2011).

[43]F. Böhm, A. Zakharova, E. Schöll, and K. Lüdge, "Amplitude-phase coupling drives chimera states in globally coupled laser networks," Phys. Rev. E **91**, 040901 (2015).

[44]R. Lhermerout, N. Bruot, G. M. Cicuta, J. Kotar, and P. Cicuta, "Collective synchronization states in arrays of driven colloidal oscillators," New J. Phys. **14**, 105023 (2012).

[45]G. L. Giorgi, F. Galve, G. Manzano, P. Colet, and R. Zambrini, "Quantum correlations and mutual synchronization," Phys. Rev. A **85**, 052101 (2012).

[46]M. Gonzalo, G. Fernando, G. G. Luca, H.-G. Emilio, and Z. Roberta, "Synchronization, quantum correlations and entanglement in oscillator networks," Sci. Rep. **3**, 1439 (2013).